

Serine and arginine rich splicing factor 1-regulated microtubule interacting and trafficking domain containing 1 affects colorectal cancer progression and ferroptosis

YULI HU¹, JIE ZHANG¹, YA LIN¹, YI LIN¹, RUI JIN¹, QIANQIAN ZHU¹ and YI MA²

¹Department of Pathology, Wenling First People's Hospital, Wenling, Zhejiang 317500;

²Department of Pathology, Sanmen People's Hospital, Taizhou, Zhejiang 317100, P.R. China

Received June 29, 2023; Accepted September 19, 2023

DOI: 10.3892/etm.2023.12334

Abstract. As the third most common type of cancer globally, colorectal cancer (CC) is a prevalent digestive malignancy, with the second highest mortality rate among all types of cancer. It has been reported that microtubule interacting and trafficking domain containing 1 (MITD1) serves a pivotal role in the initiation and progression of diverse types of tumors. Nevertheless, the underlying mechanism of MITD1 in CC has not been previously investigated. The ENCORI and GEPIA databases were used to investigate the expression levels of MITD1 in patients with CC. Immunohistochemistry was used to detect the expression of MITD1 in cancer tissues obtained from patients with CC, while its mRNA and protein expression levels in CC cell lines were determined by reverse transcription-quantitative PCR and western blot analysis, respectively. Subsequently, MITD1 was knocked down in CC cells using an interference plasmid and Cell Counting Kit 8, colony formation, as well as EdU assays were performed to assess cell proliferation. Concurrently, wound healing and Transwell assays were performed to evaluate the migration and invasion abilities of CC cells. Lipid reactive oxygen species (ROS) levels were determined by BODIPY 581/591 C11 staining. In addition, the levels of oxidative stress markers and those of total iron were measured using the corresponding kits. Furthermore, the association between serine and arginine rich splicing factor 1 (SRSF1) and MITD1 was verified by RNA immunoprecipitation and actinomycin D experiments. Finally, to further uncover the mechanism of MITD1, SRSF1 was over-expressed and MITD1 was silenced in CC cells. The results

demonstrated that the expression of MITD1 was abnormally elevated in CC tissues and CC cell lines. MITD1 silencing distinctly diminished CC cell viability, increased CC cell ferroptosis and attenuated their invasion and migration abilities. In addition, MITD1 knockdown significantly increased the expression of lipid ROS and total iron levels in CC cells. Additionally, the results showed that SRSF1 could stabilize MITD1 mRNA expression in CC cells. Finally, it was revealed that SRSF1 could regulate MITD1 and affect the progression of CC and ferroptosis via p53/solute carrier family 7 member 11 (SLC7A11)/glutathione peroxidase 4 (GPX4) signaling. Overall, the results of the current study indicated that SRSF1-regulated MITD1 could affect CC progression and ferroptosis, probably via the p53/SLC7A11/GPX4 signaling pathway.

Introduction

As the third most common type of cancer worldwide, colorectal cancer (CC) is a prevalent digestive malignancy, with the second highest mortality rate (1). In 2022, ~590,000 new cases of CC were diagnosed in China, with an upward trend (2). Surgical treatment and neoadjuvant chemotherapy are widely used to treat CC (3). However, the surgical indications are strictly limited and the quality of life of a large proportion of patients with low rectal cancer is seriously affected following surgery (4). Therefore, studying the pathogenesis of CC is of great importance.

Microtubule interacting and trafficking domain containing 1 (MITD1) encodes a protein that regulates endosomal sorting complexes required for transport III protein activity and is required for normal cell division. In addition, it has been reported that MITD1 is involved in cytokinesis (5). A previous study suggested that MITD1 dysregulation could promote tumorigenesis and gene instability, especially when it coincided with oncogene-induced mitotic stress (6). Another study demonstrated that long non-coding RNA (lncRNA) SLC16A1-AS1 knockdown downregulated MITD1 and promoted the progression of hepatocellular cancer via regulating the micro-RNA (miR)-411/MITD1 axis (7). MITD1 expression is markedly strengthened in renal clear cell carcinoma. Therefore, MITD1 silencing could mediate

Correspondence to: Dr Yi Ma, Department of Pathology, Sanmen People's Hospital, 15 Taihe Road, Hailun Street, Sanmen, Taizhou, Zhejiang 317100, P.R. China
E-mail: mayi@zjmyy.com

Key words: serine and arginine rich splicing factor 1, microtubule interacting and trafficking domain containing 1, progression, ferroptosis, colorectal cancer, p53/solute carrier family 7 member 11/glutathione peroxidase 4 signaling pathway

tafazzin (TAZ)/solute carrier family 7 member 11 (SLC7A11) pathway-induced ferroptosis to inhibit the growth and migration of clear cell renal cell carcinoma cells (8). However, the effects of MITD1 on CC and its underlying mechanism on ferroptosis have not been reported, to the best of the authors' knowledge.

Therefore, the present study aimed to investigate the role and regulatory mechanism of MITD1 in CC, thus providing a useful theoretical basis for the clinical treatment of CC.

Materials and methods

Clinical tumor tissues. CC tumor and adjacent normal tissues were obtained from Wenling First People's Hospital (Zhejiang, China). A total of 20 patients diagnosed with CC at Wenling First People's Hospital between June 2022 and December 2022 were enrolled in the present study. This group comprised 11 males and 9 females, with an average age of 35±9 years. The samples were formalin-fixed, paraffin-embedded and sectioned for the immunohistochemistry (IHC) assay according to the manufacturer's instructions. All patients provided informed written consent and the study was approved by the local institutional medical ethics review boards of Wenling First People's Hospital (approval no. KY-2023-2005-01).

Databases. The Encyclopedia of RNA Interactomes (ENCORI) database (<http://starbase.sysu.edu.cn/index.php>) was used to predict the expression levels of MITD1 in patients with CC (9). In addition, the Gene Expression Profiling Interactive Analysis (GEPIA) database (<http://gepia.cancer-pku.cn/>) was used to predict the association between the expression of MITD1 with the overall survival of patients with CC (10).

IHC assay. Following sectioning at 4 μm and deparaffinization, the paraffin-embedded tissue specimens were rehydrated in gradient ethanol. Antigen retrieval was performed in 10 mM citrate at 95°C for 20 min. Following blocking in goat serum (cat. no. R37624; Thermo Fisher Scientific, Inc.), the tissue specimens were first incubated with MITD1 antibody (cat. no. 17264-1-AP; 1:50 dilution; Proteintech) overnight at 4°C and then with the corresponding secondary antibody (cat. no. 30000-0-AP; 1:500 dilution; Proteintech) for 1 h at room temperature. After hematoxylin counterstaining for 2 min at room temperature and dehydration, images of the tissue sections in three randomly selected fields of view were captured under a light microscope (magnification, x200).

Cell culture. The normal intestinal epithelial cell line HIEC (cat. no. MZ-0792; Ningbo Mingzhou Biotechnology Co., Ltd.) and the CC cell lines Caco2 (cat. no. B164108), SW480 (cat. no. MZ-3240; both from Ningbo Mingzhou Biotechnology Co., Ltd.) and HCT116 (cat. no. BNCC287750; BeNa Culture Collection) were cultured in RPMI-1640 medium (Gibco; Thermo Fisher Scientific, Inc.) supplemented with 10% FBS (Gemini Bio Products) at 37°C in an incubator with 5% CO₂.

Reverse transcription-quantitative (RT-q) PCR. Prior to DNase I treatment, total RNA was extracted from cells (1x10⁴ cells) using the RNeasy Mini Kit (Qiagen GmbH) according to the manufacturer's instructions. The total RNA

was then reverse transcribed into cDNA using a cDNA Synthesis kit (Thermo Fisher Scientific, Inc.) according to the manufacturer's instructions. The qPCR experiments were performed using SYBR-Green reagents (Takara Bio, Inc.) according to the manufacturer's instructions. The thermocycling condition used for qPCR were as follows: 95°C for 3 min (enzyme activation), followed by 40 cycles at 95°C for 20 sec (denaturation), 60°C for 20 sec (primer annealing) and 72°C for 20 sec (extension). The mRNA expression levels were quantified using the comparative CT method (11) and GAPDH served as the calibrator gene. The PCR primers used were as follows: MITD1 forward, 5'-GTGCTAAAGCGGGCAGTAGA-3' and reverse, 5'-CAGCAGGAACCAGCTCCTTT-3', SRSF1 forward, 5'-GTTGTCTCTGGACTGCCTCC-3' and reverse, 5'-ACTTGGACAACCTTGCCTGA-3' and GAPDH forward, 5'-AATGGGCAGCCGTTAGGAAA-3' and reverse, 5'-GCGCCCAATACGACCAAATC-3'. The experiments were replicated three times.

Cell Counting Kit 8 (CCK-8) assay. Cells were seeded into a 96-well plate at a density of 2x10³ cells/well. Following induction with the corresponding compound, cells were supplemented with 10 μl CCK-8 reagent (Dojindo Molecular Technologies, Inc.) and incubated for 4 h. Finally, the absorbance at a wavelength of 450 nm was measured in each well at 24, 48 and 72 h.

Western blot analysis. Following homogenization of A549 cells in RIPA buffer (Auragene), the protein concentration was quantified using a bicinchoninic acid kit (BCA; Beyotime Institute of Biotechnology). Subsequently, 30 μg protein extracts were separated by 12% SDS-PAGE and were then transferred onto PVDF membranes. Following blocking with 5% BSA (Thermo Fisher Scientific, Inc.) for 2 h, the membranes were first incubated with primary antibodies (all from Proteintech) targeting MITD1 (cat. no. 17264-1-AP; 1:1,000 dilution), E-cadherin (cat. no. 20874-1-AP; 1:20,000 dilution), N-cadherin (cat. no. 22018-1-AP; 1:2,000 dilution), Snail (cat. no. 13099-1-AP; 1:1,000 dilution), SRSF1 (cat. no. 12929-2-AP; 1:1,000 dilution), p53 (cat. no. 60283-2-Ig; 1:5,000 dilution), p21 (cat. no. 10355-1-AP; 1:1,000 dilution), SLC7A11 (cat. no. 26864-1-AP; 1:1,000 dilution), GPX4 (cat. no. 30388-1-AP; 1:1,000 dilution) or GAPDH (cat. no. 10494-1-AP; 1:5,000 dilution) at 4°C overnight and then with the corresponding secondary antibody (cat. no. ab6721; 1:5,000 dilution; Abcam) at room temperature for 1 h. An ECL kit (MilliporeSigma) was applied to visualize blots. ImageJ software (version 1.42; National Institutes of Health) was employed for band quantification.

Cell transfection. HCT116 cells were transfected with 50 nM serine and arginine rich splicing factor 1 (SRSF1) overexpression plasmid (Oe-SRSF1) and negative control vector (Oe-NC), small hairpin RNAs (shRNAs) targeting SRSF1 (sh-SRSF1#1 or sh-SRSF1#2), shRNAs targeting MITD1 (sh-MITD1#1 or sh-MITD1#2) and the scrambled NCs (sh-NC) at 37°C for 48 h, all purchased from Shanghai GeneChem Co., Ltd., using Lipofectamine® RNAiMAX (Thermo Fisher Scientific, Inc.), according to the manufacturer's protocol. At 48 h following transfection, the cell transfection efficiency was assessed

with RT-qPCR and western blot. The target sequence of sh-MITD1#1 was 5'-TTGGATAGAAGATCCTTATAT-3'; sh-MITD1#2 was 5'-TGGATAGAAGATCCTTATATT-3'; sh-SRSF1#1 was 5'-GTGGAAGTTGGCAGGATTTAA-3'; sh-SRSF1#2 was 5'-TGGAAAGTTGGCAGGATTTAAA-3'; shRNA-NC, 5'-CAACAAGATGAAGAGCACCAA-3'.

Cell colony formation assay. Following incubation for two weeks in 6-well plates (density, 200 cells/well), cells were treated with 3.7% paraformaldehyde at room temperature for 15 min, followed by staining with 0.1% crystal violet at room temperature for 30 min. Finally, colonies with a diameter of >0.05 mm were recorded and analyzed.

EdU staining. Following HCT116 cell treatment with the indicated compounds in 6-well plates (density, 4x10⁴ cells/well), cells were immobilized, blocked and treated with EdU stain at 37°C for 2 h (Wuhan Servicebio Technology Co., Ltd.). Nuclear staining was performed for 30 min at room temperature with Hoechst dye 33342 (Beijing Solarbio Science and Technology Co., Ltd.). Images were captured under a fluorescence microscope (DMI8; Leica Microsystems GmbH).

Invasion assay. Treated cells resuspended in 200 μ l serum-free medium were added to the upper chamber of the Transwell insert pre-coated with Matrigel[®] (BD Biosciences) at 37°C for 1 h. The bottom chamber was supplemented with complete medium. Cells invading the lower chamber were immediately fixed by methanol for 48 h at 37°C, prior to staining with 0.1% crystal violet solution at room temperature for 10 min. Cell morphology was observed under an optical microscope.

Wound healing assay. Cells were seeded into 6-well plates at a density of 4x10⁴ cells/well and wounds were created on the cell nanolayer using a 200- μ l pipette tip. Following cell washing and incubation for 24 h in serum-free medium, images of the wounded gaps were captured at different time points (0 h and 24 h).

Detection of lipid reactive oxygen species (ROS) levels. The lipid ROS levels were determined using the BODIPY 581/591 C11 kit (Thermo Fisher Scientific, Inc.). Cells were seeded into 6-well plates at a density of 4x10⁴ cells/well and were then treated with 2 μ M C11-BODIPY (581/591) probe, according to the manufacturer's instructions. The cells were visualized using a fluorescent inverted microscope. Image J software (version 1.42; National Institutes of Health) was used for analysis.

Glutathione (GSH) and malondialdehyde (MDA) content. GSH and MDA levels were detected using the corresponding GSH (cat. no. S0053) and MDA (cat. no. S0131M; both from Beyotime Institute of Biotechnology) assay kits, according to the manufacturer's instructions.

Iron assays. The total iron concentrations in HCT116 cells were assessed using an iron assay kit (cat. no. ab83366; Abcam), according to the manufacturer's instructions. Following the indicated treatment, the cell supernatant was isolated after centrifugation at 16,000 x g at room temperature for 10 min

and was then supplemented with the iron probe, followed by incubation at 25°C for 1 h in the dark. The absorbance at a wavelength of 593 nm was measured using a microplate reader.

RNA immunoprecipitation (RIP) assay. RIP assay was performed using the corresponding RNA Immunoprecipitation Kit (BersinBio), according to the manufacturer's instructions. HCT116 cells (1x10⁷ cells) were lysed in RIPA lysis buffer. Following the lysis, 100 μ l cell lysates incubated with RIPA buffer containing magnetic beads conjugated with 1 μ g anti-MITD1 (cat. no. 17264-1-AP; 0.5 μ g; Proteintech) or 2 μ g IgG (cat. no. 30000-0-AP; 0.5 μ g; Proteintech) at 4°C overnight. Subsequently, proteinase K buffer was applied for the digestion of the protein from samples and the immunoprecipitated RNA was extracted using TRIzol reagent (Invitrogen; Thermo Fisher Scientific, Inc.). After purification, the precipitated RNA was analyzed by RT-qPCR analysis as aforementioned.

Actinomycin D assay. To evaluate the stability of linear RNA, the transcription of RNA was inhibited following cell treatment with 1 μ g/ml actinomycin D (MedChemExpress) or DMSO (control) for 0, 3, 6, 9 and 12 h. RNA was then extracted for RT-qPCR analysis as aforementioned.

Statistical analysis. All data were analyzed by SPSS software (version 20.0; IBM Corp.). All results are expressed as the mean \pm standard deviation. Intergroup comparison of the mean values was implemented employing one-way ANOVA followed by Tukey's post-hoc test. P<0.05 was considered to indicate a statistically significant difference.

Results

MITD1 is upregulated in CC. The ENCORI database showed that MITD1 was highly expressed in tumor tissues derived from patients with CC (Fig. 1A). Additionally, the GEPIA database demonstrated that elevated MITD1 expression was notably associated with lower overall survival in patients with CC (Fig. 1B). IHC staining showed that the expression of MITD1 in cancer tissues from patients with CC was abnormally elevated (Fig. 1C). In addition, the mRNA and protein expression levels of MITD1 in different CC cell lines were detected by RT-qPCR and western blot analysis, respectively. The results showed that compared with HIEC cells, MITD1 was significantly upregulated in CC cell lines. More specifically, the expression levels of MITD1 were more notably increased in HCT116 cells. Therefore, HCT116 cells were selected for the subsequent experiments (Fig. 1D).

MITD1 knockdown attenuates CC cell proliferation and metastasis. A MITD1 interference plasmid was constructed and the transfection efficiency was evaluated via RT-qPCR and western blot analysis. Since MITD1 expression was more notably reduced in the sh-MITD1#2 group compared with the sh-MITD1#1 group, sh-MITD1#2 was selected for the follow-up experiments (Fig. 2A). CCK-8, colony formation and EdU staining assays revealed that compared with the sh-NC group, cell viability and proliferation were markedly diminished in the sh-MITD1 group (Fig. 2B-D). Additionally,

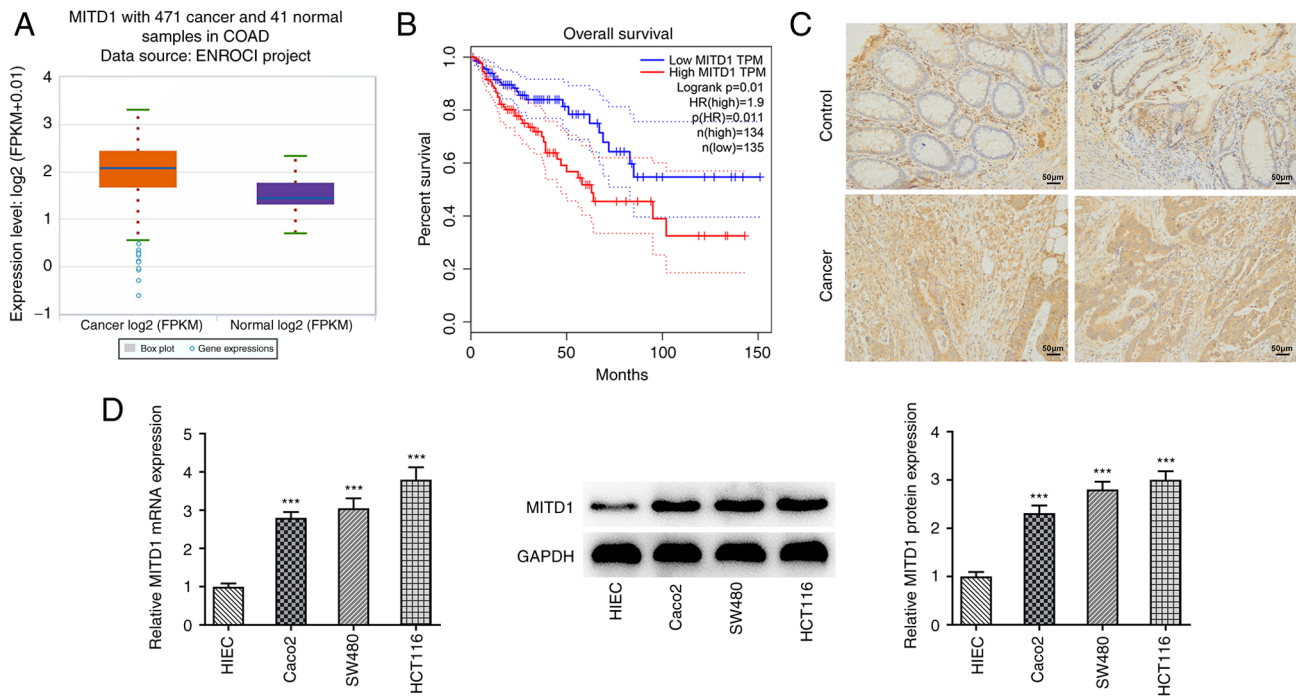


Figure 1. MITD1 is upregulated in CC. (A) The expression profile of MITD1 in CC tumor tissues was downloaded from the ENCORI database. (B) The association between MITD1 expression and the prognosis of patients with CC was predicted using the GEPIA database. (C) Immunohistochemistry assay was performed to detect MITD1 expression in CC tissues (magnification, x200). (D) The expression levels of MITD1 in different CC cell lines were detected by reverse transcription-quantitative PCR and western blot analysis. *** $P < 0.001$ vs. HIEC cells. MITD1, microtubule interacting and trafficking domain containing 1; CC, colorectal cancer.

the wound healing and Transwell assay results elaborated that the invasion and migration capacities of CC cells were distinctly attenuated following MITD1 silencing (Fig. 2E and F). Furthermore, western blot analysis was performed to detect the expression levels of epithelial-to-mesenchymal transition (EMT)-related proteins. The results showed that E-cadherin was upregulated and N-cadherin and Snail were downregulated in MITD1-depleted CC cells (Fig. 2G).

MITD1 interference promotes ferroptosis in CC cells. BODIPY (581/591) C11 staining was used to determine the levels of lipid ROS. The experimental data showed that lipid ROS content was markedly increased in the sh-MITD1 group compared with the sh-NC group (Fig. 3A). In addition, compared with the sh-NC group, GSH generation was declined and MDA content was enhanced in the sh-MITD1 group (Fig. 3B). Finally, total iron levels were detected using the corresponding kit and the results showed that they were significantly increased following MITD1 silencing (Fig. 3C).

SRSF1 stabilizes MITD1 mRNA. RT-qPCR and western blot analysis revealed that the expression levels of SRSF1 were abnormally elevated in CC cell lines (Fig. 4A). RIP assay verified the binding capability of SRSF1 with MITD1 mRNA (Fig. 4B). Subsequently, SRSF1 was silenced and overexpressed separately, and the transfection efficiency was assessed by RT-qPCR and western blot analysis. The results demonstrated that cells were successfully transfected (Fig. 4C). Subsequently, RT-qPCR showed that following SRSF1 knockdown in cells treated with actinomycin D, the stability of MITD1 mRNA was significantly decreased (Fig. 4D). Furthermore, SRSF1

silencing could significantly inhibit the expression of MITD1 in CC cells, while SRSF1 overexpression exerted the opposite effect (Fig. 4E).

SRSF1 regulates MITD1 to affect the progression and ferroptosis of CC via p53/SLC7A11/GPX4 signaling. Subsequently, MITD1 was silenced and SRSF1 was overexpressed in CC cells, concurrently. The CCK-8 results showed that cell viability in the sh-MITD1 + Oe-SRSF1 group was notably increased compared with the sh-MITD1 + Oe-NC group (Fig. 5A). Colony formation and EdU staining assays indicated that the proliferation capacity of CC cells in the sh-MITD1 + Oe-SRSF1 group was overtly enhanced compared with the sh-MITD1 + Oe-NC group (Fig. 5B and C). Additionally, wound healing and Transwell assays showed that the simultaneous SRSF1 overexpression and MITD1 silencing significantly enhanced the invasion and migration abilities of CC cells (Fig. 5D and E). Western blot analysis suggested that compared with the sh-MITD1 + Oe-NC group, E-cadherin expression declined, while that of N-cadherin and Snail was elevated in the sh-MITD1 + Oe-SRSF1 group (Fig. 5F). Furthermore, following SRSF1 overexpression and MITD1 knockdown, lipid ROS and MDA contents were prominently reduced, while those of GSH were notably enhanced (Fig. 6A and B). In addition, total iron levels were also apparently decreased (Fig. 6C). Finally, western blot analysis was performed to detect the expression levels of proteins involved in the p53/SLC7A11/GPX4 signaling pathway. The results demonstrated that p53 and p21 were noticeably upregulated in the sh-MITD1 group compared with the control group. However, SLC7A11 and GPX4 were evidently downregulated.

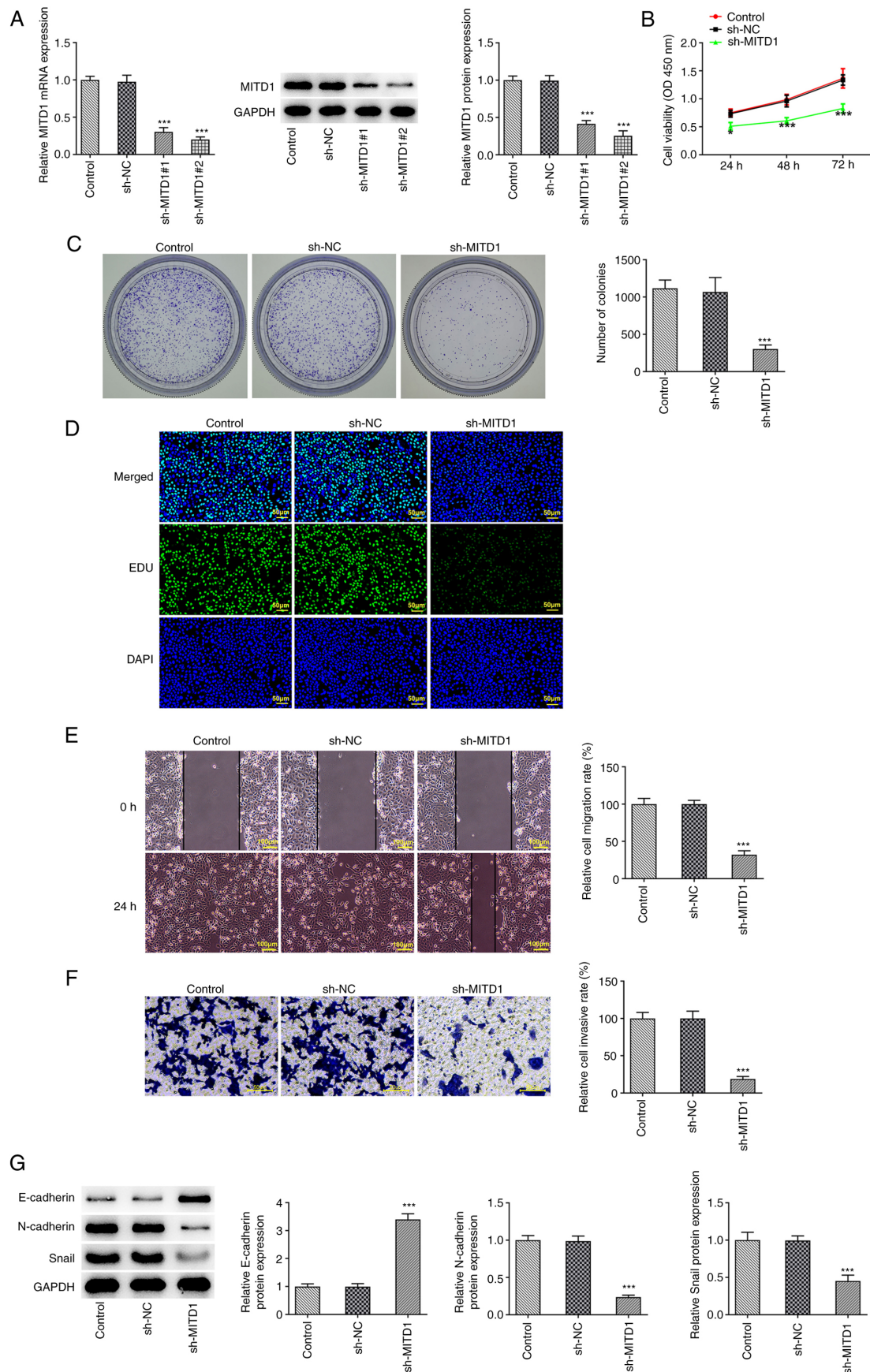


Figure 2. MITD1 silencing inhibits CC cell proliferation and metastasis. (A) The transfection efficiency of CC cells with MITD1 interference plasmids was assessed by reverse transcription-quantitative PCR and western blot analysis. (B) A Cell Counting Kit 8 assay was performed to evaluate cell activity. The cell proliferation ability was also assessed by (C) colony formation and (D) EdU staining assays (scale bars, 50 μ m). (E) Wound healing (scale bars, 100 μ m) and (F) Transwell assays (scale bars, 50 μ m) were applied to determine cell migration and invasion. (G) The expression levels of epithelial-to-mesenchymal transition-related proteins were detected by western blot analysis. * $P < 0.05$ and *** $P < 0.001$ vs. the sh-NC group. MITD1, microtubule interacting and trafficking domain containing 1; CC, colorectal cancer; sh, small hairpin; NC, negative control.

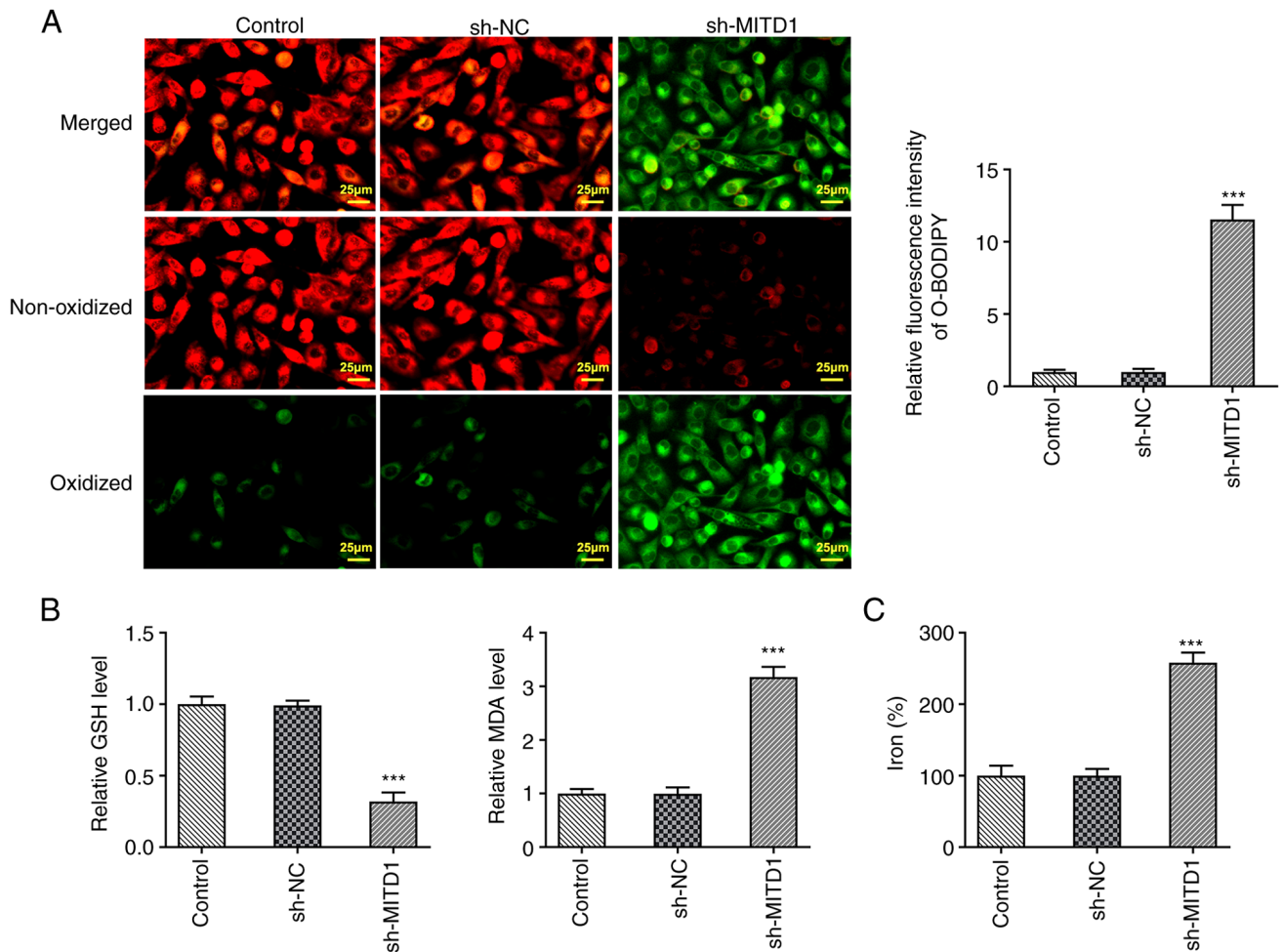


Figure 3. MITD1 overexpression promotes ferroptosis in colorectal cancer cells. (A) BODIPY (581/591) C11 staining was used to determine the levels of lipid reactive oxygen species (scale bars, 25 μ m). (B) Glutathione and malondialdehyde contents were measured using the corresponding kits. (C) Total iron levels were determined using the corresponding kit. *** $P < 0.001$ vs. the sh-NC group. MITD1, microtubule interacting and trafficking domain containing 1; sh, small hairpin; NC, negative control; GSH, glutathione; MDA, malondialdehyde.

Compared with the sh-MITD1 + Oe-NC group, the expression levels of the p53/SLC7A11/GPX4 signaling pathway-related proteins were partially reversed in the sh-MITD1 + Oe-SRSF1 group (Fig. 6D).

Discussion

Although the current diagnostic and treatment approaches for CC are constantly improving, the 5-year survival rate remains <12%, suggesting the extremely poor prognosis of patients with CC diagnosed at advanced stages (12). Therefore, understanding the initiation and progression of CC is of great importance for providing particular insights into the clinical diagnosis and treatment of CC.

In the present study, bioinformatics analysis using the ENCORI database revealed that MITD1 was upregulated in CC tissues. Additionally, the GEPIA database also suggested that increased MITD1 expression was closely associated with low overall survival rate of patients with CC. Emerging evidence has suggested that MITD1 can be considered as a molecular marker for predicting the prognosis of several types of cancers, including hepatocellular carcinoma and renal cell carcinoma (6,13). However, the expression and

mechanism of MITD1 in CC have not been previously investigated to the best of the authors' knowledge. The results of the present study demonstrated that the expression levels of MITD1 were increased in CC tumor tissues compared with adjacent normal tissues. Furthermore, MITD1 expression was also abnormally elevated in CC cell lines, highlighting the potential of MITD1 as a prognostic marker for CC. To elucidate the specific regulatory effect of MITD1 on CC growth, MITD1 was silenced. The results showed that CC cell proliferation, invasion and migration were notably decreased. The above findings were consistent with the results reported by Chen *et al* (14), demonstrating that MITD1 knockdown could significantly inhibit bladder cancer cell migration and proliferation.

In recent years, relevant clinical studies have suggested that ferroptosis has significant translational research potential for the occurrence, development and clinical treatment of several types of malignant tumors (15,16). A previous study showed that tagitinin C could induce ferroptosis via the protein kinase RNA-like ER kinase/nuclear factor-erythroid 2-related factor 2/heme oxygenase-1 signaling pathway in CC cells, ultimately suppressing CC growth (17). N-acetyltransferase 10 could promote colon

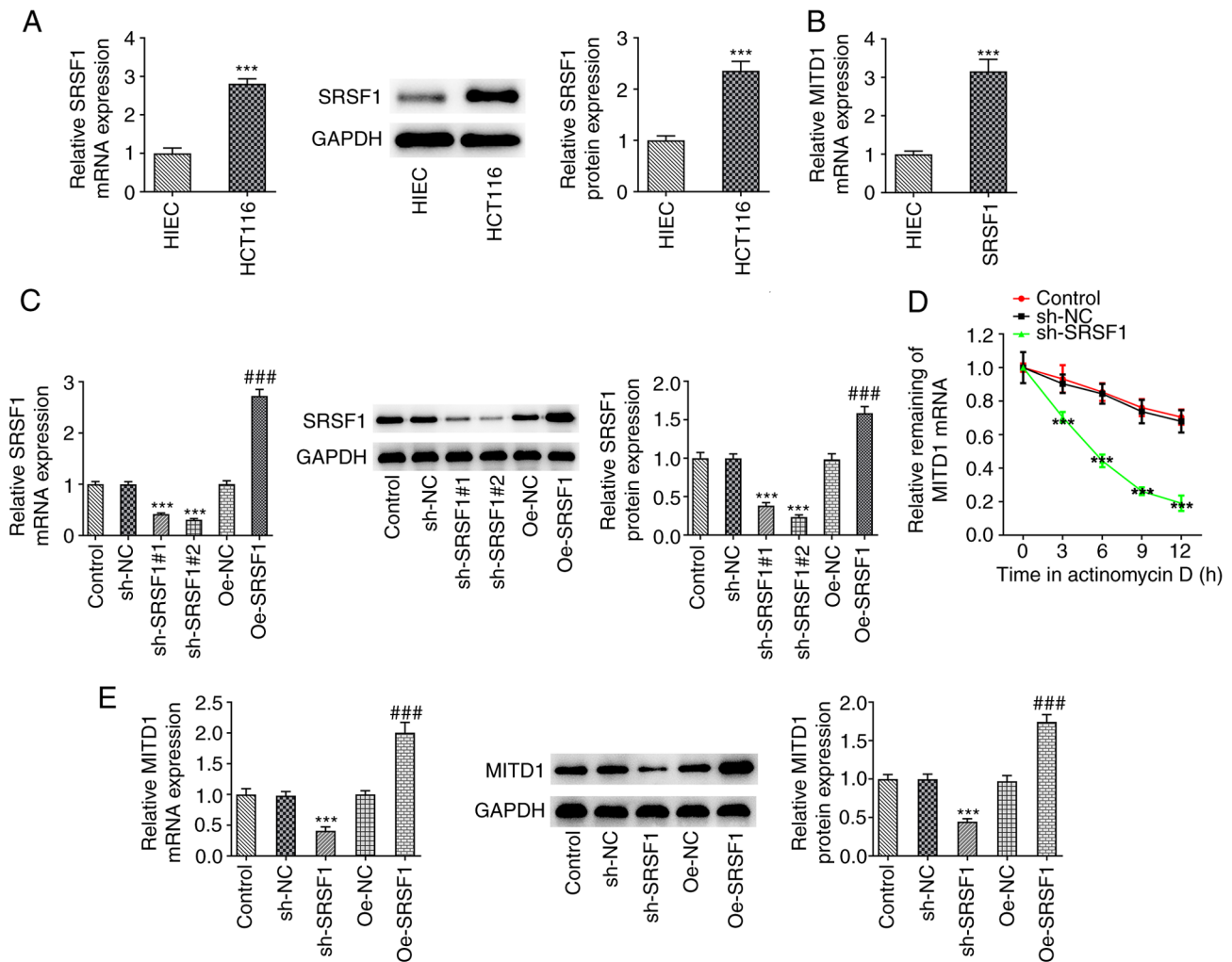


Figure 4. SRSF1 stabilizes MITD1 mRNA. (A) The SRSF1 mRNA and protein expression levels were detected in CC cell lines using RT-qPCR and western blot analysis, respectively. *** $P < 0.001$ vs. HIEC cells. (B) RNA immunoprecipitation assays were performed to evaluate the binding capacity of SRSF1 with MITD1 mRNA. *** $P < 0.001$ vs. the Control group. (C) The transfection efficiency of CC cells with shRNAs targeting SRSF1 and SRSF1 overexpression plasmids was determined via RT-qPCR and western blot analysis. (D) The stability of MITD1 mRNA was assessed by RT-qPCR. *** $P < 0.001$ vs. the sh-NC group. (E) The mRNA and protein expression levels of MITD1 were detected using RT-qPCR and western blot analysis, respectively. *** $P < 0.001$ vs. the sh-NC group; ### $P < 0.001$ vs. the Oe-NC group. SRSF1, serine and arginine rich splicing factor 1; MITD1, microtubule interacting and trafficking domain containing 1; CC, colorectal cancer; RT-qPCR, reverse transcription-quantitative PCR; sh, small hairpin; NC, negative control; Oe, overexpression.

cancer progression via inhibiting ferroptosis through N4-acetylation and stabilization of ferroptosis suppressor protein 1 mRNA (18). Therefore, inducing ferroptosis in tumor cells could be considered as a novel strategy for the clinical treatment of malignant tumors. In the current study, MITD1 silencing promoted ferroptosis in CC cells. Consistent with the above results, a previous study revealed that MITD1 knockdown could induce ferroptosis and inhibit tumor growth and migration via the TAZ/SLC7A11 signaling pathway in clear cell renal cell carcinoma (8).

In the present study, the ENCORI database was used to predict the potential interaction between the RNA binding protein SRSF1 and MITD1. In addition, the regulatory interaction between SRSF1 and MITD1 in CC cells was verified by relevant experiments. A previous study showed that SRSF1 could prevent DNA damage and promote colon cancer via regulating DBF4B pre-mRNA splicing (19). LncRNA AGAP2-AS1 targeted the miR-4668-3p/SRSF1 axis to exacerbate CC cell proliferation, migration, invasion and EMT (20).

Another study also showed that propofol could downregulate circular RNA PABPN1, upregulate miR-638 or downregulate SRSF1 in a dose-dependent manner to inhibit the development of CC (21). In the current study, SRSF1 expression was aberrantly increased in CC cells. Therefore, it was hypothesized that SRSF1 could be involved in cell viability, migration and invasion via activating MITD1 expression. Another study demonstrated that LINC01564 could promote the resistance of glioma cells to temozolomide via binding with SRSF1. Additionally, LINC01564 promoted the mRNA stability of mitogen-activated protein kinase 8 (MAPK8) via recruiting SRSF1, thus promoting the MAPK8/nuclear factor (erythroid derived 2) like 2 phosphorylation and inhibiting ferroptosis in glioma cells. Overall, the study suggested that LINC01564 and SRSF1 could inhibit ferroptosis in glioma cells (22). In the present study, SRSF1 overexpression reversed the activation of ferroptosis in CC cells following MITD1 knockdown.

A previous study showed that MITD1 knockdown inhibited the TAZ/SLC7A11 pathway and induced ferroptosis, while

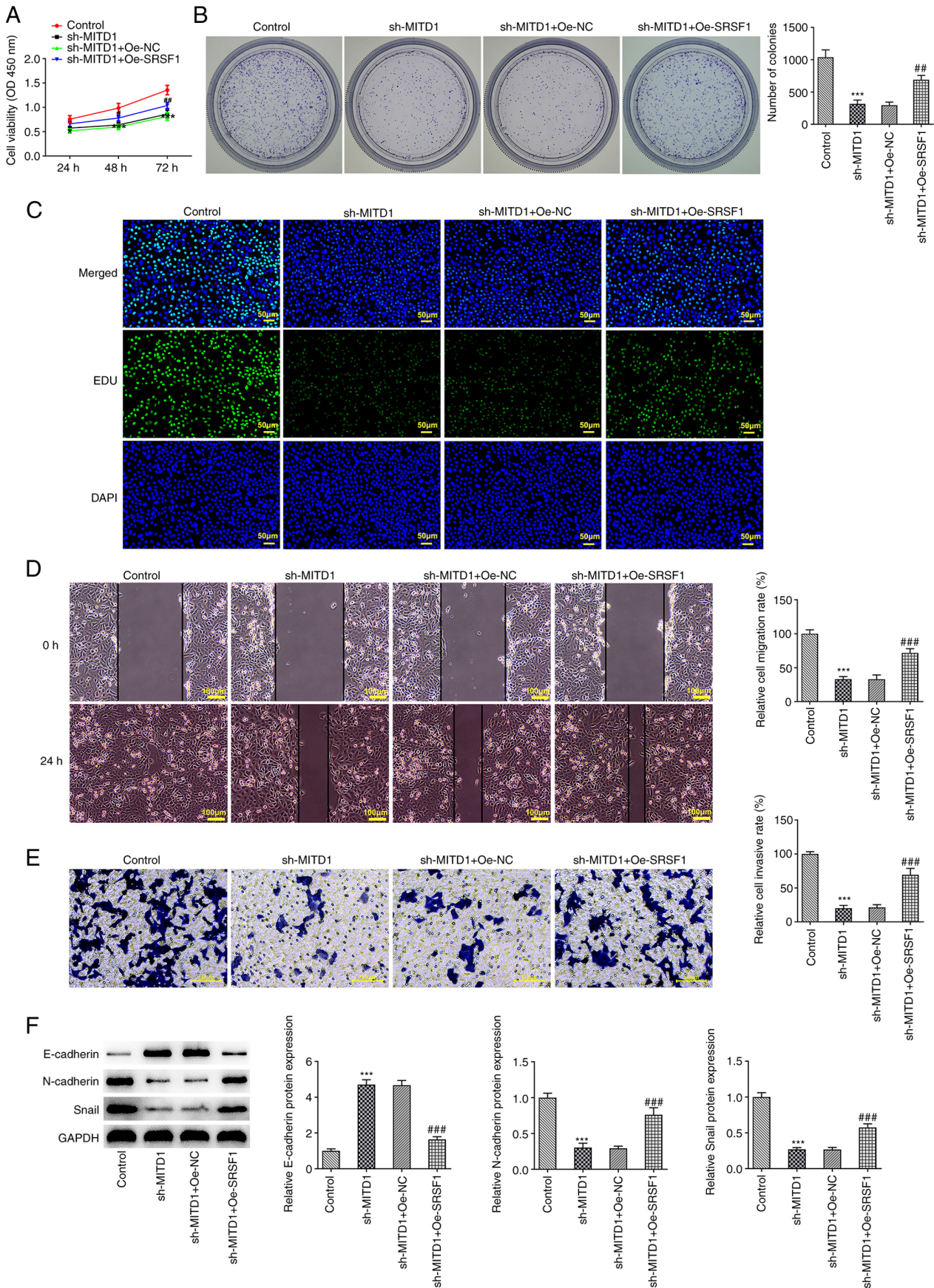


Figure 5. SRSF1 regulates MITD1 to affect the progression of CC via p53/solute carrier family 7 member 11/glutathione peroxidase 4 signaling. (A) Cell viability was assessed by Cell Counting Kit 8 assay. The proliferation ability of CC cells was evaluated using (B) colony formation and (C) EdU assays (scale bar, 50 μ m). (D) Wound-healing (scale bar, 100 μ m) and (E) Transwell assays (scale bar, 50 μ m) were performed to assess cell migration and invasion. (F) The expression levels of epithelial-to-mesenchymal transition-related proteins were detected using western blot analysis. *** $P < 0.001$ vs. the sh-NC group; ** $P < 0.01$, ### $P < 0.001$ vs. the Oe-NC group. SRSF1, serine and arginine rich splicing factor 1; CC, colorectal cancer; MITD1, microtubule interacting and trafficking domain containing 1; sh, small hairpin; NC, negative control; Oe, overexpression.

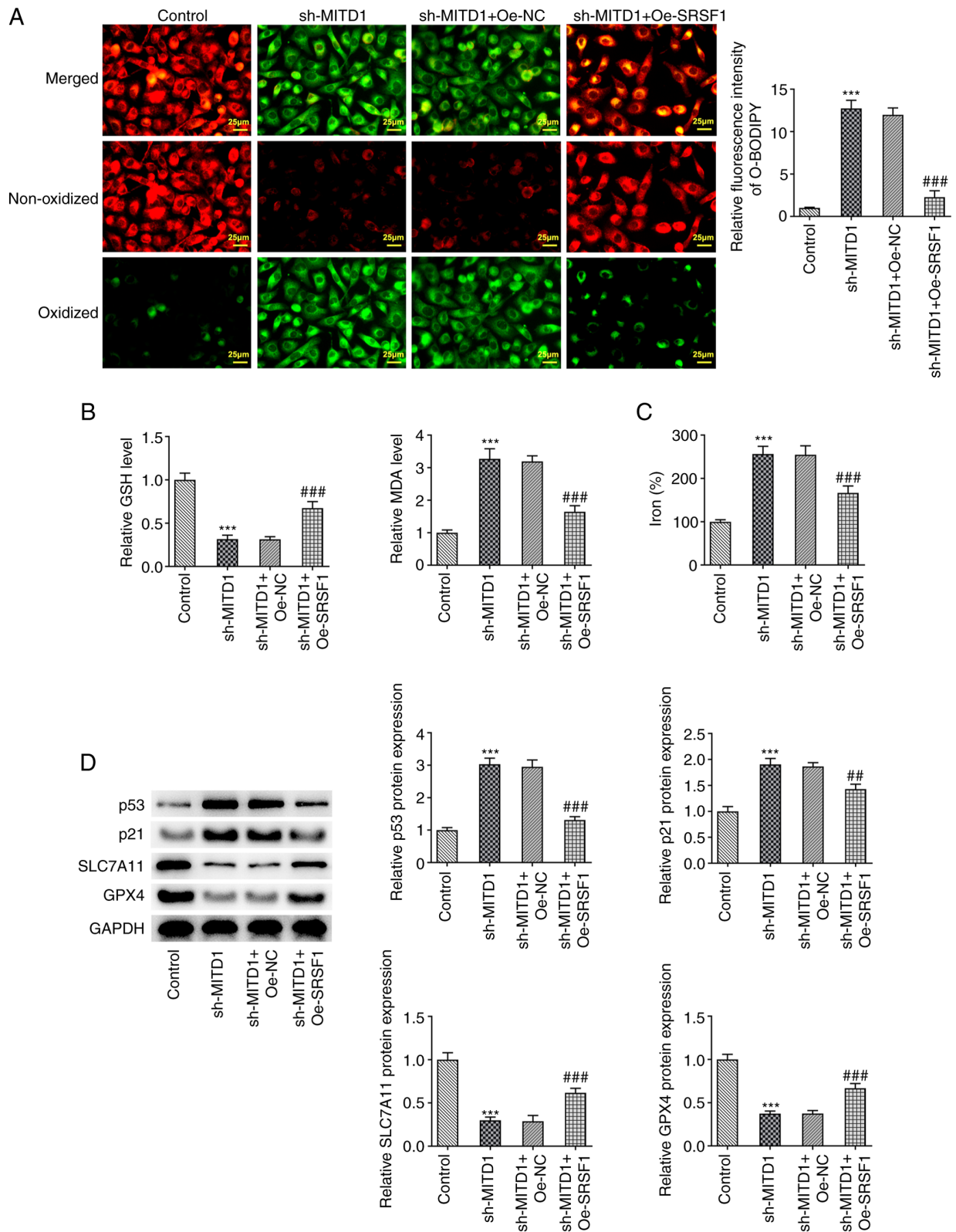


Figure 6. SRSF1 regulates MITD1 to affect ferroptosis in colorectal cancer cells via p53/SLC7A11/GPX4 signaling. (A) Lipid reactive oxygen species levels were measured by BODIPY (581/591) C11 staining (scale bar, 25 μ m). (B) GSH and MDA contents were measured using the corresponding kits. (C) Total iron levels were detected using the corresponding kit. (D) The expression levels of p53/SLC7A11/GPX4 signaling-related proteins were detected using western blot analysis. *** P <0.001 vs. the sh-NC group; ## P <0.01, ### P <0.001 vs. the sh-MITD1 + Oe-NC group. SLC7A11, solute carrier family 7 member 11; GPX4, glutathione peroxidase 4; SRSF1, serine and arginine rich splicing factor 1; CC, colorectal cancer; MITD1, microtubule interacting and trafficking domain containing 1; GSH, glutathione; MDA, malondialdehyde; GPX4, glutathione peroxidase 4; sh, small hairpin; NC, negative control; Oe, overexpression.

TAZ could block the inhibition of p53 and enhance cancer cell proliferation (8,23). In addition, shank-associated RH domain

interactor promoted the proliferation of bile duct carcinoma cells and inhibited ferroptosis via p53/SLC7A11/GPX4

signaling (24). By interacting with SRSF1, lncRNA-626 could inactivate the p53 pathway to exert its oncogenic activity in gastric cancer (25). Therefore, it was reasonable to hypothesize that MITD1 regulated by SRSF1 could affect the growth of CC via p53/SLC7A11/GPX4 signaling. The present study showed that MITD1 silencing in CC cells could promote the activation of p53 and p21 expression and members of the p53/SLC7A11/GPX4 signaling pathway and downregulate SLC7A11 and GPX4. The expression levels of the p53/SLC7A11/GPX4-related proteins were further reversed by SRSF1 overexpression. These results indicated that SRSF1 could regulate MITD1 and affect CC progression and ferroptosis and this process may be achieved by modifying the regulation of p53/SLC7A11/GPX4 signaling. Future experiments will further explore the regulatory mechanism by adding p53/SLC7A11/GPX4 pathway activators or pathway inhibitors.

Overall, the results of the present study suggested that SRSF1-regulated MITD1 could affect the progression and ferroptosis in CC, which may be via the p53/SLC7A11/GPX4 signaling pathway.

Acknowledgements

Not applicable.

Funding

The present study was supported by the Wenling City social development science and technology project (grant no. 2022S00155).

Availability of data and materials

The datasets generated and/or analyzed during the present study are available from the corresponding author on reasonable request.

Authors' contributions

YM, YH and JZ wrote the manuscript and analyzed the data. YaL, YiL, RJ and QZ performed the experiments and supervised the study. YM searched the literature, and revised the manuscript for important intellectual content. YH and YM confirmed the authenticity of all the raw data. All authors have read and approved the final manuscript.

Ethics approval and consent to participate

All experimental procedures were approved by the Wenling First People's Hospital (Zhejiang, China; approval no. KY-2023-2005-01) and all patients provided written informed consent to participate.

Patient consent for publication

Not applicable.

Competing interests

The authors declare that they have no competing interests.

References

- Keum N and Giovannucci E: Global burden of colorectal cancer: Emerging trends, risk factors and prevention strategies. *Nat Rev Gastroenterol Hepatol* 16: 713-732, 2019.
- Xia C, Dong X, Li H, Cao M, Sun D, He S, Yang F, Yan X, Zhang S, Li N and Chen W: Cancer statistics in China and United States, 2022: Profiles, trends, and determinants. *Chin Med J (Engl)* 135: 584-590, 2022.
- Dekker E, Tanis PJ, Vleugels JLA, Kasi PM and Wallace MB: Colorectal cancer. *Lancet* 394: 1467-1480, 2019.
- Cayrol C and Girard JP: Interleukin-33 (IL-33): A nuclear cytokine from the IL-1 family. *Immunol Rev* 281: 154-168, 2018.
- Lee S, Chang J, Renvoisé B, Tipirneni A, Yang S and Blackstone C: MITD1 is recruited to midbodies by ESCRT-III and participates in cytokinesis. *Mol Biol Cell* 23: 4347-4361, 2012.
- Shen H, Wang Z, Ren S, Wang W, Duan L, Zhu D, Zhang C and Duan Y: Prognostic biomarker MITD1 and its correlation with immune infiltrates in hepatocellular carcinoma (HCC). *Int Immunopharmacol* 81: 106222, 2020.
- Duan C: LncRNA SLC16A1-AS1 contributes to the progression of hepatocellular carcinoma cells by modulating miR-411/MITD1 axis. *J Clin Lab Anal* 36: e24344, 2022.
- Zhang Y, Li Y, Qiu Q, Chen Z, Du Y and Liu X: MITD1 deficiency suppresses clear cell renal cell carcinoma growth and migration by inducing ferroptosis through the TAZ/SLC7A11 pathway. *Oxid Med Cell Longev* 2022: 7560569, 2022.
- Li JH, Liu S, Zhou H, Qu LH and Yang JH: starBase v2.0: Decoding miRNA-ceRNA, miRNA-ncRNA and protein-RNA interaction networks from large-scale CLIP-Seq data. *Nucleic Acids Res* 42: D92-D97, 2014.
- Li C, Tang Z, Zhang W, Ye Z and Liu F: GEPIA2021: Integrating multiple deconvolution-based analysis into GEPIA. *Nucleic Acids Res* 49: W242-W246, 2021.
- Livak KJ and Schmittgen TD: Analysis of relative gene expression data using real-time quantitative PCR and the 2(-Delta Delta C(T)) method. *Methods* 25: 402-408, 2001.
- Health Commission Of The People's Republic Of China N: National guidelines for diagnosis and treatment of colorectal cancer 2020 in China (English version). *Chin J Cancer Res* 32: 415-445, 2020.
- Chen C and Sheng Y: Prognostic impact of MITD1 and associates with immune infiltration in kidney renal clear cell carcinoma. *Technol Cancer Res Treat* 20: 15330338211036233, 2021.
- Chen Y, Xu T, Xie F, Wang L, Liang Z, Li D, Liang Y, Zhao K, Qi X, Yang X and Jiao W: Evaluating the biological functions of the prognostic genes identified by the pathology atlas in bladder cancer. *Oncol Rep* 45: 191-201, 2021.
- Kong N, Chen X, Feng J, Duan T, Liu S, Sun X, Chen P, Pan T, Yan L, Jin T, *et al*: Baicalin induces ferroptosis in bladder cancer cells by downregulating FTH1. *Acta Pharm Sin B* 11: 4045-4054, 2021.
- Liang Y, Zhang L, Peng C, Zhang S, Chen S, Qian X, Luo W, Dan Q, Ren Y, Li Y and Zhao B: Tumor microenvironments self-activated nanoscale metal-organic frameworks for ferroptosis based cancer chemodynamic/photothermal/chemo therapy. *Acta Pharm Sin B* 11: 3231-3243, 2021.
- Wei R, Zhao Y, Wang J, Yang X, Li S, Wang Y, Yang X, Fei J, Hao X, Zhao Y, *et al*: Tagitinin C induces ferroptosis through PERK-Nrf2-HO-1 signaling pathway in colorectal cancer cells. *Int J Biol Sci* 17: 2703-2717, 2021.
- Zheng X, Wang Q, Zhou Y, Zhang D, Geng Y, Hu W, Wu C, Shi Y and Jiang J: N-acetyltransferase 10 promotes colon cancer progression by inhibiting ferroptosis through N4-acetylation and stabilization of ferroptosis suppressor protein 1 (FSP1) mRNA. *Cancer Commun (Lond)* 42: 1347-1366, 2022.
- Chen L, Luo C, Shen L, Liu Y, Wang Q, Zhang C, Guo R, Zhang Y, Xie Z, Wei N, *et al*: SRSF1 prevents DNA damage and promotes tumorigenesis through regulation of DBF4B Pre-mRNA splicing. *Cell Rep* 21: 3406-3413, 2017.
- Li H, Guo S, Zhang M, Li L, Wang F and Song B: Long non-coding RNA AGAP2-AS1 accelerates cell proliferation, migration, invasion and the EMT process in colorectal cancer via regulating the miR-4,668-3p/SRSF1 axis. *J Gene Med* 22: e3250, 2020.
- Zhao A and Liu Y: Propofol suppresses colorectal cancer development by the circ-PABPN1/miR-638/SRSF1 axis. *Anal Biochem* 631: 114354, 2021.

22. Luo C, Nie C, Zeng Y, Qian K, Li X and Wang X: LINC01564 promotes the TMZ resistance of glioma cells by upregulating NFE2L2 expression to inhibit ferroptosis. *Mol Neurobiol* 59: 3829-3844, 2022.
23. Miyajima C, Hayakawa Y, Inoue Y, Nagasaka M and Hayashi H: HMG-CoA reductase inhibitor statins activate the transcriptional activity of p53 by regulating the expression of TAZ. *Pharmaceuticals (Basel)* 15: 1015, 2022.
24. Zeng C, Lin J, Zhang K, Ou H, Shen K, Liu Q, Wei Z, Dong X, Zeng X, Zeng L, *et al*: SHARPIN promotes cell proliferation of cholangiocarcinoma and inhibits ferroptosis via p53/SLC7A11/GPX4 signaling. *Cancer Sci* 113: 3766-3775, 2022.
25. Wu ZH, Liu CC, Zhou YQ, Hu LN and Guo WJ: OnclncRNA-626 promotes malignancy of gastric cancer via inactivated the p53 pathway through interacting with SRSF1. *Am J Cancer Res* 9: 2249-2263, 2019.



Copyright © 2023 Hu et al. This work is licensed under a Creative Commons Attribution-NonCommercial-NoDerivatives 4.0 International (CC BY-NC-ND 4.0) License.